Spectroscopy and Dynamics of Al Atoms Solvated in Superfluid Helium Nanodroplets†

James H. Reho, Udo Merker, Matthew R. Radcliff, Kevin K. Lehmann, and Giacinto Scoles*

Department of Chemistry, Princeton University, Princeton, New Jersey 08544

Received: October 26, 1999; In Final Form: February 23, 2000

The laser-induced fluorescence excitation spectrum in the vicinity of the $3^2D \leftarrow 3^2P$ transition of Al atoms solvated in superfluid helium nanodroplets has been measured. While this transition has not been studied in bulk liquid helium, the observed blue shifts and line broadenings, compared with other transitions for which such measurements do exist, allow us to conclude that Al atoms reside in the interior of the helium droplet. The observed transition shows a splitting that we attribute to quadrupole-like deformations of the cavity formed in the helium droplet around the Al atom. Time-resolved studies of wavelength-selected emission from solvated Al atoms excited to the 3^2D state reveal a rapid ($\leq$50 ps) and seemingly total nonradiative population transfer to the 4^2S state, the decay of which is found to account for all of the emission and to have a lifetime (6.4 ± 0.1 ns) that matches that of gas-phase Al.

Introduction

Probe atoms attached to or solvated in helium nanodroplets have proven to be a sensitive tool for investigating the properties of both the dopant atoms and the ultracold, superfluid helium droplets themselves.[1,2] The liquid helium droplets offer a rather weakly perturbative matrix in comparison with solid matrixes, the effects of which can be probed spectroscopically. While it is known that alkali atoms and their dimers reside as surface species on helium nanodroplets,[3,4] studies of alkali atoms seeded into bulk liquid helium by laser sputtering techniques[5] have allowed for solvation studies of these simple, hydrogen-like probes. Explanation of the spectroscopic data from these studies necessitates the inclusion of spin−orbit interactions. Spectra obtained in the region of the D_1 lines ($nP_{1/2} \leftarrow nS_{1/2}$) of Rb and Cs can be simulated by use of the bubble model,[6] in which Pauli repulsion between the helium bath and the alkali atoms produces a spherical cavity inside the helium. The dual-component profiles of the spectra taken in the region of the D_2 lines ($nP_{3/2} \leftarrow nS_{1/2}$) of the same dopants are attributed instead to quadrupole-like deformations of the bubble.[6] Thus, different spin−orbit components of the same electronic state elicit quite different behaviors from the helium bath.

Spin−orbit effects have also been observed in the formation dynamics of Na−He[7] and K−He[8] exciplexes on the surface of liquid helium droplets. In these studies, the differing exciplex formation dynamics are found to be dependent on which spin−orbit component of the *n*P state of the alkali atom is combined with He. While the extraction of a He atom from the droplet plays a significant role in the dynamics of this process, the measurable difference in exciplex formation rate after excitation of different spin−orbit states of the alkali atom has been quantitatively modeled on the basis of spin−orbit mixing induced by the helium bath.[8] The same type of phenomenon has also been studied for Ag solvated in liquid helium,[9,10] in which spin−orbit decoupling of the AgHe electronic states is required in order to explain the dynamics of AgHe and $AgHe_n$ formation in the bulk liquid.

A second type of phenomenon that has been found to occur in the interaction of the solute atoms with the helium bath is the opening of nonradiative decay channels. As an example, deformation of the cavity in the helium bath, caused by the presence of the dopant atom, has also been proposed for the case of electronically excited Na atoms in bulk liquid helium.[11] In this case, it is thought that from four to six helium atoms fall into a ring around the excited 3^2P Na atom in the nodal plane perpendicular to the occupied p orbital. This ring is then thought to open nonradiative relaxation channels from both the $3^2P_{3/2}$ and $3^2P_{1/2}$ levels to the ground state of the atom because of curve crossing with the strongly repulsive ground-state potential.[12] Such channels are thought to account for the absence of fluorescence from atomic Li and Na solvated in bulk liquid helium.[13] Similarly, the nonstatistical intensity ratios between the two D lines of the larger alkali atoms in bulk liquid helium[14] are thought to arise due to nonradiative transitions between different spin−orbit states brought about by the helium.

In this context, the use of atoms with electronic ground states with partially filled p electron shells[15] (such as Al) may serve to deepen our understanding. We have thus undertaken the study of the spectra and dynamics of Al atoms solvated in liquid helium droplets. The study of Al, in which the gas-phase spin−orbit splitting (112 cm^{-1}) is of the order of the depth of the dopant-He_n potential well, allows for a direct probe of the competing energetics between spin−orbit mixing and the solvation forces responsible for the quenching mechanisms induced by the helium. We note here that spectra of Al in solid Ar, Kr, and Xe matrixes[16−19] and in neat methane[20] have been previously investigated, including a recent prediction of the $AlAr_n$ spectrum by Monte Carlo techniques.[21] Comparison of our results with the results from these more traditional matrixes are presented below. We also present comparisons of our Al−He $1^2\Pi_{1/2}$ potential surfaces with prior studies of the $1^2\Pi_{1/2}$ surfaces of Al with other (Ne, Ar, Kr, and Xe) rare gas atoms.

A further point that should be emphasized at this point is that when spin−orbit decoupling does occur, barriers toward oligomer formation are often the result. As mentioned above, AgHe,[9] $AgHe_2$,[10] and alkali atom−He exciplex[7,8] formation rates differ according to which spin−orbit component is excited. Particularly, formation along the $1^2\Pi_{1/2}$ surface is delayed due to the presence of a barrier that occurs due to the $1^2\Pi_{1/2}-1^2\Sigma_{1/2}$

† Part of the special issue "Marilyn Jacox Festschrift".

10.1021/jp9937961 CCC: $19.00
Published on Web 04/01/2000

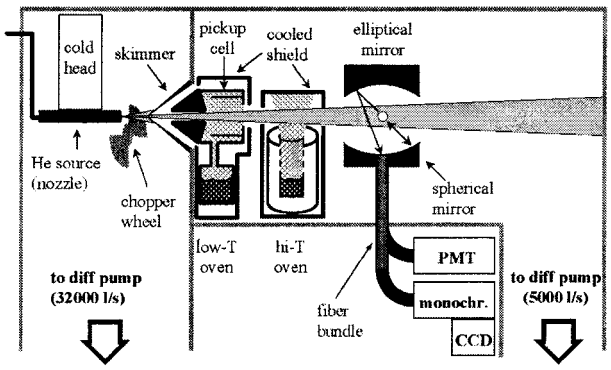

Figure 1. Experimental apparatus used for studying helium nanodroplets containing seeded atoms.

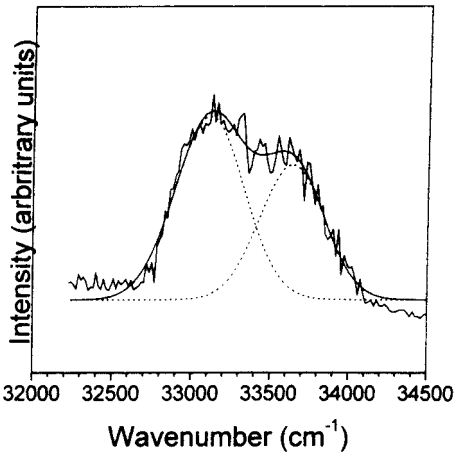

Figure 2. $3^2D \leftarrow 3^2P$ transitions of Al atoms solvated in helium nanodroplets. The fit to the spectrum (solid line) is a summation of two Gaussian line shapes (dotted lines).

interaction. Precise knowledge of such low-lying (several cm^{-1}) barriers, such as may be present in the recombination of two Al atoms or in the reaction of Al atoms with other spherical light dopants (such as Li), is also relevant to increasing the efficacy of solid propellants.[22] The existence of such barriers to atom−atom recombination would allow for higher concentrations of light metal dopants in solid hydrogen, improving the properties of this material as a rocket propellant.

Experimental Section

A detailed description of the apparatus used in our laboratory for the production of helium nanodroplets has been given before.[3] Here a summary description will be given, highlighting recent enhancements that have made possible the pickup of low vapor pressure dopants by the helium droplets. The new configuration of our apparatus is shown schematically in Figure 1.

Large He nanodroplets ($\langle N \rangle \sim 10^3-10^4$) are produced by the free jet expansion of He gas with a stagnation pressure of 2.5 MPa through a 20 μm nozzle held at a temperature of 17 K. After collimation by a 400 μm skimmer, the droplets are doped with Al atoms from our high-temperature vapor source. This source is composed of a high-temperature vacuum deposition furnace run by a power controller (LUXÉL RADAK II). Temperatures up to 1770 K can be attained in this source. The cylindrical furnace, of 20 mm diameter, is surrounded by a water-cooled Cu covering to minimize scattered light from blackbody radiation and to collect the evaporated metal. This shield has two 5 mm holes through which the helium beam can pass and is connected to the chamber by a home-built Cu platform.

After the pick-up of atomic vapor, the helium nanodroplets are probed by laser light about 220 mm from the nozzle. The laser beam intersects the molecular beam perpendicularly at the center of a laser-induced fluorescence detector composed of a spherical and elliptical mirror. Note that the spherical mirror is omitted in the collection of time-resolved spectra.[7] The laser-induced fluorescence is focused onto a multimode, incoherent fiber bundle and is brought to a microchannel plate detector (Hammamatsu R2807U-07), the output of which is amplified. In the collection of frequency-resolved spectra with pulsed lasers, this signal is then processed by a boxcar integrator with a gate width of 25 ns. The exiting laser beam itself, after crossing the molecular beam, is detected by a photomultiplier tube or a fast photodiode and is likewise processed by a boxcar integrator.

The time-resolved spectra are collected using time-correlated single photon counting. In our photon counting apparatus, described in detail elsewhere,[7] the signal arising from the microchannel plate detector and the signal arising from the correlated laser pulse impinging on a fast photodiode are processed by a constant fraction discriminator (Tennelec TC454). The output signals of the discriminator are sent to an EG&G Ortec time-to-amplitude converter (TAC). The output of the TAC is processed by a Nucleus PCA II multichannel analyzer that contains 8192 channels. The multichannel analyzer is set to cover a 320 ns region of time, and the photon counting instrument itself has a time resolution[23] of 50 ps.

The laser light used in these studies is generated in the Center for Ultrafast Laser Applications (CULA) located in the Department of Chemistry of Princeton University in a facility just above our laboratory. The system centers around a Ti:sapphire laser (Spectra Physics Tsunami) mode-locked at 80 MHz that is regeneratively amplified by means of a Spectra-Physics Spitfire amplifier and then further enhanced by a double-pass unit located within the latter. The amplifier is pumped with two Spectra-Physics Merlin YLF lasers and puts out a pulse train with a repetition rate of 1 kHz at a wavelength of 800 nm. This output is frequency-doubled to pump a Light Conversion TOPAS optical parametric amplifier. The TOPAS output is doubled by passage through a BBO crystal, yielding the final laser light output that is continuously tunable from 235 to 400 nm. Typical pulse energies of 5 μJ per pulse (i.e., 5 mW average power) are measured at the entrance to our molecular beam apparatus. The spectral width of the laser pulses was determined by scanning the $3^1 P_1{}^0 \leftarrow 3^1 S_0$ gas-phase transition of atomic Mg, and for the present studies has been measured to have a fwhm of 25 cm^{-1}. The frequency of the TOPAS amplifier is calibrated against the spectral lines of an Fe−Ne hollow cathode lamp through use of the optogalvanic effect.

Excitation Spectra

The spectrum of the $3^2D \leftarrow 3^2P$ excitation of Al atoms attached to helium droplets is shown in Figure 2. This spectrum is blue-shifted by roughly 1000 cm^{-1} from the known gas-phase positions of the $3^2D_{3/2} \leftarrow 3^2P_{1/2}$ and $3^2D_{5/2} \leftarrow 3^2P_{3/2}$ transitions (32 435 and 32 325 cm^{-1}, respectively[24]). The large blue shift and broadening can be taken as evidence of the solvation of Al in the helium droplet. While we report here the first observation made using nanodroplets of the $3^2D \leftarrow 3^2P$ transitions of Al in liquid helium, similar broadening has been observed for the $4^2S \leftarrow 3^2P$ transition of Al in bulk liquid helium.[14] The even larger blue shift (2600 cm^{-1}) of the latter (bulk) transition is most likely due to a stronger repulsion between the Al electron

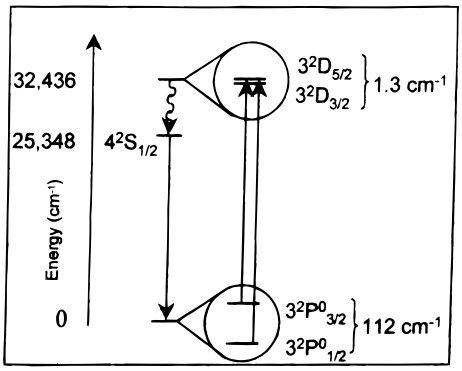

Figure 3. Energy level diagram of Al, highlighting the splitting of the 3^2P and 3^2D levels. The straight arrows correspond to optical excitation and emission mentioned in the text while the wavy arrow corresponds to the nonradiative quenching discussed in the text.

TABLE 1: Parameters of the Two Gaussians Representing the Best Fit to the Spectrum of Al Atoms Solvated in Helium Droplets As Depicted in Figure 2

Gaussian	center (cm^{-1})	fwhm (cm^{-1})	rel area (%)
I	$33\,111 \pm 15$	436 ± 22	59 ± 5
II	$33\,635 \pm 19$	408 ± 27	41 ± 5

cloud and the helium cavity upon excitation into the more extended 4^2S state compared to excitation to the 3^2D state.

From earlier work in the gas phase[24] it has been established that the splitting between the $3^2P_{3/2}$ and $3^2P_{1/2}$ (ground) states of Al is 112 cm^{-1}, while the splitting between the $3^2D_{3/2}$ and $3^2D_{5/2}$ states of Al is only 1.3 cm^{-1} (cf. Figure 3). The splitting between the $3^2D_{5/2}$ and $3^2D_{3/2}$ states of Al is irresolvable given the width of our laser pulses (25 cm^{-1} fwhm), while the $3^2P_{3/2}$ and $3^2P_{1/2}$ splitting in Al should be resolvable. However, as seen in Figure 2, the observed splitting is much larger (524 cm^{-1}) and no structural feature with the predicted splitting is found in the spectrum although the oscillator strengths of the $3^2D_{3/2} \leftarrow 3^2P_{1/2}$ and $3^2D_{5/2} \leftarrow 3^2P_{3/2}$ transitions (0.18 and 0.16, respectively) are nearly the same. The oscillator strength of the $3^2D_{3/2} \leftarrow 3^2P_{3/2}$ transition is about 10 times weaker[24] than the preceding two transitions. However, in light of the fast (nanosecond or subnanosecond) relaxation among the spin−orbit states in the case of alkali atoms solvated in bulk liquid helium,[14] we do in fact expect complete relaxation to the lower ($3^2P_{1/2}$) spin−orbit level, as the time between Al atom pickup and probing is on the order of 100 μs.

The measured spectrum was fit with two Gaussian line shapes, as illustrated in Figure 2. These Gaussians and the resultant fit are shown in the figure as dotted and solid lines, respectively. Parameters from the best fit to the data are given in Table 1. As the observed splitting is much larger than the gas-phase $3^2P_{3/2}-3^2P_{1/2}$ level separation, we have performed calculations (cf. below) that indicate the orbital angular momentum in the 3^2P state is quenched by the helium matrix due to the strongly anisotropic interactions with the helium. As mentioned in the Introduction, nonradiative $n^2P_{3/2} \rightarrow n^2P_{1/2}$ relaxation mechanisms have been postulated for alkali atoms in bulk liquid helium,[12] and the lack of fluorescence from the $5^2P_{3/2}$ level of Rb atoms embedded in bulk liquid helium has been attributed to such relaxation mechanisms.[25]

Dual-component profiles similar to that observed above in the spectrum of Al solvated in He droplets have been observed by Kinoshita et al.[6] following D_2 ($n^2P_{3/2} \leftarrow n^2S_{1/2}$) excitation of Cs ($n = 6$) and Rb ($n = 5$) atoms in bulk liquid helium. These authors reach a qualitative understanding of their data by developing a deformed bubble model in which oscillatory quadrupole deformations of the cavity surrounding the alkali atom dopant split the degenerate atomic state. As the $3^2D \leftarrow 3^2P$ transition of Al picked up by He clusters exhibits the same qualitative features as the $n^2P_{3/2} \leftarrow n^2S_{1/2}$ spectra of Cs and Rb in bulk liquid helium obtained by Kinoshita et al., it is reasonable to postulate that similar quadrupole-like deformations of the helium cavity produce the characteristic spectral splitting observed in our experiment. In our case, however, the distortion of the cavity is already present in the initial state (3^2P) of the transition.

In comparing our excitation spectrum with the Al spectroscopy done in matrixes of other noble gases, it is found that the 3-fold splitting of the $3^2D \leftarrow 3^2P$ absorption of Al atoms induced by Ar, Kr, and Xe matrixes span 700, 1300, and 1000 cm^{-1}, respectively.[18] This 3-fold splitting stands in contrast to the dual-component profile induced by the helium described above, which has a span of only 524 cm^{-1} between the two maxima. The ~2500 cm^{-1} blue shift of the Al $3^2D \leftarrow 3^2P$ transition in Ar from the gas-phase frequency is found to be more than double that induced by the helium nanodroplet, measured at ~1000 cm^{-1} (see above). The Al $3^2D \leftarrow 3^2P$ transition measured in a Kr matrix gives one component red-shifted by 160 cm^{-1} and two that are blue-shifted from the gas-phase position by 565 and 1129 cm^{-1}. While the intensity positions in Kr average closest to the gas-phase position (even in comparison with the nanodroplet spectrum), this result cannot be taken as a lessening of matrix perturbation as the spread in position of the three components of the $3^2D \leftarrow 3^2P$ transition are greatest in Kr. The Xe matrix induces red shifts of ~1500 cm^{-1} for the three frequency components. Thus, the matrix-induced blue shift brought about in Al by solvation in helium nanodroplets is most closely mirrored by the Ar, while Kr and Xe matrixes give rise to Al intensities that are progressively more red-shifted from those brought about by Ar. The dual-component profile of Al in helium nanodroplets discussed above shows that the droplets offer smaller matrix perturbation in comparison with the wide 3-fold matrix-induced splitting of the $3^2D \leftarrow 3^2P$ Al transition induced by Ar, Kr, and Xe.

The Al−He Potential Energy Surface and Spin−Orbit Mixing

The $(X)1^2\Pi$ and $1^2\Sigma$ potential energy surfaces of AlHe have been calculated using the Hartree−Fock damped dispersion (HFD) ansatz,[26] a widely used semiempirical method that has been found to be quite accurate for atom combinations involving species of the first and second row of the periodic table.[26,27]

This method describes the potential energy surface in terms of two components, one of which (ΔE_{SCF}) is the Hartree−Fock self-consistent field energy and is assumed to contain all uncorrelated contributions. The correlation energy is instead represented by a damped multipole expansion constructed on the basis of available dispersion coefficients (ΔE_{corr}). The HFD-generated spin−orbit-averaged $(X)1^2\Pi$ and $1^2\Sigma$ HFD potential surfaces are shown as dotted curves in Figure 4, where the energies are referred to the Al($[Ne]3s^23p^1$) + He($2s^2$) asymptote. The ΔE_{SCF} component was calculated in the 6-311++G** basis using the Gaussian 94 program suite,[28] correcting for basis set superposition error at each point. The ΔE_{corr} component makes use of the AlHe C_n coefficients calculated using the AlAr C_n coefficients of LePicard et al.,[15] the Ar_2 and He_2 C_n coefficients of Standard and Certain,[29] and standard combination methods.[30] These C_n coefficients used in generating the $1^2\Pi$ and $1^2\Sigma$ AlHe HFD surfaces are given in Table 2. We note here that use of these potential energy surfaces in helium density functional

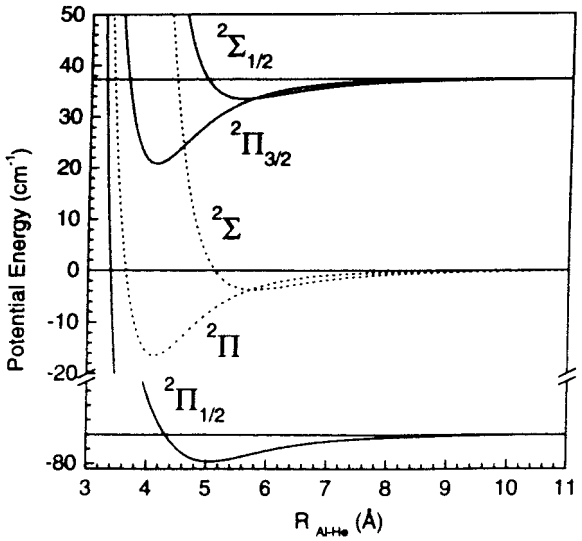

Figure 4. Spin−orbit-averaged $1^2\Sigma$ and $1^2\Pi$ and spin−orbit-decoupled $1^2\Sigma_{1/2}$, $1^2\Pi_{1/2}$, and $1^2\Pi_{3/2}$ potential energy surfaces of AlHe.

TABLE 2: C_n Coefficients Used in Generating the $1^2\Pi$ and $1^2\Sigma$ Surfaces of AlHe by Use of the HFD Ansatz[a]

parameter	$1^2\Sigma$ AlHe	$1^2\Pi$ AlHe
C_6	1.6695×10^5	8.6183×10^4
C_8	2.1140×10^6	1.0913×10^6
C_{10}	3.7354×10^7	1.9283×10^7

[a] All energies are in cm^{-1} and all distances in Å.

calculations[31] performed in our group[32] yield results consistent with the Al atom being solvated in the helium droplets, finding a 62 cm^{-1} minimum for Al occupation in the center of the droplet, as compared to a 42 cm^{-1} minimum for the Al atom on the surface of the droplet when the isotropic $1^2\Pi_{1/2}$ potential surface is used.

Spin−orbit coupling of the $1^2\Pi$ and $1^2\Sigma$ AlHe HFD surfaces yields the solid curves given in Figure 4, again with energies referred to the original Al($[Ne]3s^23p^1$) + He($2s^2$) asymptote. The procedure of spin−orbit coupling, described elsewhere in detail for the diatomic case,[7−9] involves the use of the experimental atomic spin−orbit splitting Δ_{so} (112 cm^{-1}) to approximate the magnitude of the spin−orbit operator. This distance-independent approximation is expected to be valid at long range.[7] We have appended here this Hamiltonian for the case of Al−He_n where $n \geq 3$ and the helium atoms are arranged so as to form a symmetric polygon in the *xy* plane around the Al atom:

$$\begin{bmatrix} nV_\Pi & \frac{\Delta_{SO}}{3}\sqrt{2} & 0 \\ \frac{\Delta_{SO}}{3}\sqrt{2} & \frac{n}{2}(V_\Pi + V_\Sigma) - \frac{\Delta_{SO}}{3} & 0 \\ 0 & 0 & \frac{n}{2}(V_\Pi + V_\Sigma) + \frac{\Delta_{SO}}{3} \end{bmatrix}$$

In fact, we use the six basis functions P_{+1}, P_0, P_{-1}, $\bar{P}_{+1}$, $\bar{P}_0$, $\bar{P}_{-1}$ with M_J values $+^3/_2$, $+^1/_2$, $-^1/_2$, $+^1/_2$, $-^1/_2$, $-^3/_2$ that split into two 1×1 blocks of $M_J = +^3/_2$ or $-^3/_2$ functions (i.e., P_{+1} or $\bar{P}_{-1}$) and two 2×2 blocks that contain the (P_0, $\bar{P}_{+1}$) and ($\bar{P}_0$, P_{-1}) functions. Assuming pairwise additivity, the P_0 states interact solely with nV_Π and the $P_{\pm1}$ states solely with the $(n/2)(V_\Pi + V_\Sigma)$ excluding the spin−orbit interaction. When the spin−orbit interaction is included, the $1^2\Pi$ surface is found to split into a $1^2\Pi_{1/2}$ and $1^2\Pi_{3/2}$ surface, the former of which mixes with the $1^2\Sigma_{1/2}$ state and thus has a minimum of potential at a larger internuclear distance (5.05 Å) than either the $1^2\Pi_{3/2}$ or the spin−orbit-averaged $1^2\Pi$ surface. Characteristic parameters of these surfaces are given in Table 3. The $1^2\Pi$ surface is seen to have a minimum at 4.12 Å, while the $1^2\Sigma$ minimum occurs at an AlHe distance of 5.77 Å.

TABLE 3: Parameters of the Spin−Orbit-Averaged and Spin−Orbit-Decoupled AlHe Potential Energy Surfaces As Calculated by the HFD Ansatz Including Equilibrium Internuclear Distance (R_{min}), Well Depth (ϵ), and Zero of Potential (σ)[a]

Al−He surface	R_{min} (Å)	ϵ (cm^{-1})	σ (cm^{-1})
$1^2\Pi$	4.12	16.45	3.64
$1^2\Sigma$	5.77	3.74	5.10
$1^2\Pi_{3/2}$	4.12	16.42	3.64
$1^2\Pi_{1/2}$	5.05	4.97	4.32
$1^2\Sigma_{1/2}$	5.54	3.81	4.94

[a] All well depth energies and zero of potential values of the various states are referenced to their respective asymptotes.

TABLE 4: Comparison of Well Depth (ϵ) and Internuclear Distance (R_{min}) for the $1^2\Pi_{1/2}$ Surface of Al and Various Noble Gases[a]

$1^2\Pi_{1/2}$	ϵ (cm^{-1})	R_{min} (Å)
AlHe	4.97	5.05
AlNe	14 ± 0.3 (ref 33)	not given
AlAr	122.4 ± 4 (ref 34)	3.79 ± 0.01
	165^{+40}_{-10} (ref 35)	3.79 ± 0.01
	165 ± 94 (ref 36)	3.5 ± 0.2
AlKr	194.7 ± 0.8 (ref 34)	3.84 ± 0.01
	194.7 ± 0.8 (ref 37)	3.84 ± 0.01
	197 ± 90 (ref 36)	3.7 ± 0.2
AlXe	308 ± 85 (ref 36)	3.6 ± 0.2

[a] It is noted here that all ϵ values reported from ref 36 are actually the dissociation energies D_e.

We note here that the potential energy surfaces of AlNe,[33] AlAr,[34,35,36] AlKr,[34,37] and AlXe[36] have been determined from fluorescence measurements. In comparing our AlHe $1^2\Pi_{1/2}$ surface with those for Al and these other noble gas atoms, we find that our AlHe surface fits well with the trend toward increasing well depth as the noble gas atom becomes larger. The well depths ϵ and equilibrium internuclear distances R_{min} for Al and these noble gases are given in Table 4. It is found from the table that while the well depth becomes increasingly larger as the noble gas increases in size, any trend in the equilibrium internuclear distance is less evident. However, our HFD AlHe surface shows a R_{min} value of almost double those for AlAr and AlKr.

After generation of our HFD AlHe surfaces, we have used them to investigate the nature of Al electron localization for the Al−He_n system. In particular, the main question addressed here is whether the ground-state Al valence is best described by the spin−orbit-decoupled $1^2\Pi_{3/2,1/2}$ surfaces or by the spin−orbit-averaged nonspherical $1^2\Pi$ surface. In the former case, we expect only the lower-energy ($1^2\Pi_{1/2}$) spin−orbit-decoupled surface to be populated due to the cold environment of the helium droplet. The Al electron density correlating with this state is spherical. If the spin−orbit interaction is quenched in the helium, the spin−orbit-averaged $1^2\Pi$ surface, correlating with an aspheric Al electron density, would describe the Al−He_n interaction. In the latter case the electron distribution would be expected to resemble that of He around an excited (*n*P) alkali atom as discussed above. The upper frame a of Figure 5 compares the $AlHe_n$ ($n = 1$, 4, 6−8) $1^2\Pi$ potential energy surfaces based upon our $1^2\Pi_{1/2}$ AlHe HFD results used under the assumption of additivity. These surfaces are created by arranging

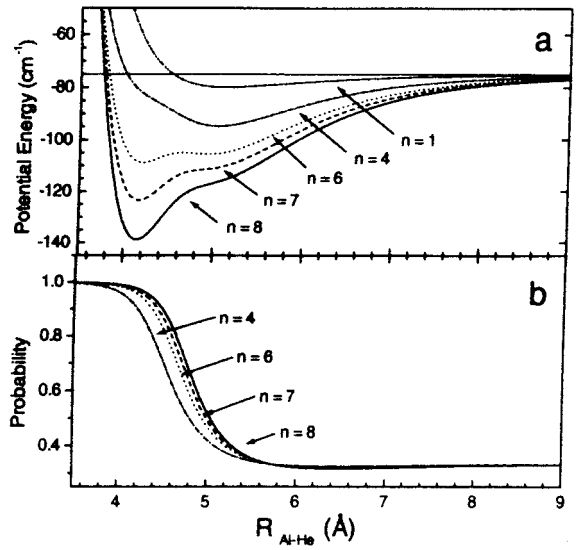

Figure 5. (a) $1^2\Pi$ potential energy surfaces of AlHe (dot-dot−dash line), $AlHe_4$ (dot−dash line), $AlHe_6$ (dotted line), $AlHe_7$ (dashed line), and $AlHe_8$ (solid line), where the helium atoms are arranged symmetrically on the *xy* plane around the Al p_z orbital. *(*b) Probability of occupation of the Al p_z orbital as a function of the Al−He distance for each of the $AlHe_n$ configurations depicted above, using the same line designations.

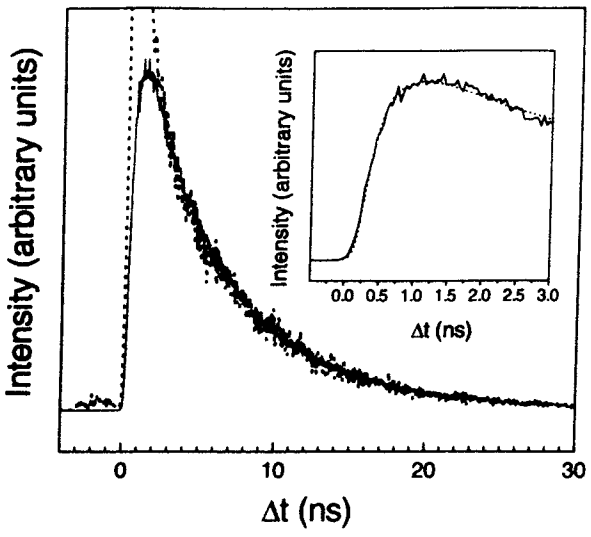

Figure 6. Dotted line: Temporally dispersed fluorescence of Al atoms upon excitations near the $3^2D \leftarrow 3^2P$ transition of Al. The rising edge is masked by scattered light. Solid line: Temporally dispersed fluorescence of Al atoms upon excitations near the $3^2D \leftarrow 3^2P$ transition of Al, detecting only frequencies near the $4^2S \rightarrow 3^2P$ transition frequency region of Al. The inset highlights this rising edge (solid curve) and the best fit to the data (dotted curve).

the helium atoms in symmetric polygons in the nodal plane around the p orbital of Al. From the figure it is seen that, in the case in which four, six, and eight He atoms have assembled around the node of the Al, a minimum appears at distances near the initial spin−orbit-averaged $1^2\Pi$ minimum (4.13 Å), while the $1^2\Pi_{1/2}$ minimum at 5.05 Å goes through a "shelf" state and almost disappears. We can thus conclude that as the number of He atoms around the node of the Al atom increases (i.e., as *n* increases), the mixing in of Σ character into the $1^2\Pi$ state, predicted by spin−orbit mixing, becomes less and less. This lack of Σ character corresponds to less and less Al valence electron density in the *xy* plane (i.e., the plane defined by the He_n polygons), affording an attractive region into which the He atoms can be drawn. Another way to view these changes in the potential energy surfaces is as representative of the localization of the Al valence electron in its p_z orbital (i.e., the Al p orbital perpendicular to the plane defined by the He atoms), which occurs to a greater extent as *n* increases. Thus, we see in Figure 5a that at $n = 4$, the minima at 5.05 Å and at 4.13 Å are of almost equal depth, while at $n = 8$ the latter has almost totally dominated the former. Thus, these additive surfaces support the conclusion that the spin−orbit decoupling is quenched in the helium solvent so that the density profile of the Al p electron takes on the aspherical p_z character.

While zero-point energy effects are not explicitly considered here, it is expected that the He density in the droplets will strongly increase in the well at 4.13 Å. Monte Carlo calculations carried out on SF_6 (the interaction of which with He is of similar magnitude as Al) indicate a high degree of such localization.[38] The quenching of the spin−orbit interaction for solvated Al atoms (and thus for an aspherical Al valence electron density) is further supported by our density functional findings[32] in which the solvation structure of Al in helium droplets indicates that the Al electron density is localized in the Al p_z orbital by yielding a high population density of He in the region of the Al *xy* nodal plane. The density functional code employed in our calculations treat the solute atom (Al) as a classical object in a quantum liquid and thus accounts for zero point motion provided the solute mass is greater than that of helium.

The lower frame b of Figure 5 shows the probability of occupation of the p_z orbital as a function of Al−He_n distance for the $AlHe_n$ ($n = 4$, 6−8) surfaces depicted in the upper frame of the figure. The distance coordinate, then, corresponds to a symmetric "breathing" of the polygonal He ring. It is found in comparing the two frames that the movement from 0.33 (spin−orbit-averaged) population of the Al p_z orbital to full (1.0) occupancy occurs in the region corresponding to the shelf in the Al−He_n surfaces, that is, in the region between the two minima. It is also found in the figure that this transition occurs "earlier", i.e., at slightly longer internuclear distance, as the number of He atoms in the node is increased. It is thus seen that spin−orbit mixing is more rapidly quenched as the number of He atoms forming the polygon (i.e., as the number of He atoms surrounding the Al on its nodal plane) increases. The He−He distance corresponding to the peak of the low-temperature pair correlation of liquid helium (3.5 Å)[39] provides the upper limit for the He−He distances of the He atoms that make up the Al-centered polygons.[40] The Al−He distance of 4.2 Å corresponds both to the AlHe $1^2\Pi$ equilibrium internuclear distance and to the position of the $AlHe_n$ ground-state minimum for $n > 4$ (cf. Figure 5). At this AlHe distance, a ring of 7(8) He atoms is found to have a He−He spacing of 3.6(3.2) Å. Thus, a polygon containing 7 He atoms exhibits He−He distances that are too large. Therefore, we conclude that at least 8 He atoms will collect around the Al atom. This has been shown above to be sufficient to quench the spin−orbit coupling.

Time-Resolved Spectra

Time-correlated single photon counting was employed in the collection of lifetime measurements of excited Al atoms solvated in helium droplets. The iterative convolution process used in generating best fits to the time-resolved spectra has been described in detail previously.[7] Here we confine ourselves only to the results. Temporal evolution of the fluorescence generated upon laser excitation of Al solvated in He droplets at 33 048 and 33 717 cm^{-1} is shown as a dashed line in Figure 6. The rising edge of this trace is masked by scattered light. Fits to the data yielded lifetimes of 6.4 ± 0.1 ns, in marked disagreement

with the known lifetimes of the $3^2D_{5/2}$ and $3^2D_{3/2}$ states (13.5 ± 0.4 ns and 13.3 ± 0.4 ns, respectively).[24] Thus, the temporally resolved emission could not be attributed to the 3^2D states of Al. A band-pass filter[41] was then introduced in order to pass only $3^2D \rightarrow 3^2P$ emission (33 333 ± 2100 cm^{-1}). Introduction of this filter prevented any fluorescence from being detected upon laser excitation at 33 048 and 33 717 cm^{-1}, confirming the fact that the Al emission corresponds to transitions other than the $3^2D \rightarrow 3^2P$.

The lifetime of the $4^2S_{1/2}$ state of Al is known to be 6.8 ± 0.7 ns,[42] which is, within the error, our measured value. Another band-pass filter[43] was introduced in order to block all $3^2D \rightarrow 3^2P$ emission and pass only $4^2S \rightarrow 4^2P$ emission (25 000 ± 1310 cm^{-1}) fluorescence. Introduction of this band-pass filter yielded substantial fluorescence, shown in Figure 6 as a solid line, which was well fit by the same 6.4 ns lifetime as in the case of the total emission collection. It becomes therefore apparent that the initially populated $3^2D_{5/2,3/2}$ states of Al are quenched to the 4^2S state on a subnanosecond time scale due to interaction with the He matrix. This entails a transfer of nearly 7100 cm^{-1} of energy into the surrounding helium. This energy corresponds to evaporation of over 1400 helium atoms from the cluster in order to reestablish the steady-state cluster temperature of 0.37 K (assuming that all 7100 cm^{-1} of energy goes into equilibrium evaporation).

The time constant fit to the onset of fluorescence passed through the $4^2S_{1/2}$ Al band-pass filter, highlighted in the inset of Figure 6, represents the time in which the nonradiative transfer of energy occurs from the 3^2D states to the 4^2S state of Al. This onset yields an instrumentally limited time constant (i.e., rise time) of 50 ± 50 ps. This fast population transfer attests to the strongly perturbative presence of the helium environment on the dynamics of electronically excited atoms, already evidenced by the spin−orbit quenching of alkali atoms in bulk liquid helium[12] and by fast nonadiabatic population transfer seen in the case of K_2 on the He droplet surface.[44]

Direct laser excitation of solvated 3^2P Al atoms to the $4^2S_{1/2}$ state has also been carried out using an excitation frequency of 27 778 cm^{-1}. The same experimental lifetime of 6.4 ± 0.1 ns has been obtained by fits to this temporally dispersed emission. These temporally resolved spectra exactly reproduce those collected upon $3^2D \leftarrow 3^2P$ excitation of solvated Al within our temporal resolution of ±50 ps and, together with our selective emission experiments, confirm the hypothesis made above.

Conclusions

The combination of low vapor pressure metal sources and ultraviolet laser light has provided the opportunity to probe the interaction of Al atoms with helium nanodroplets. This paper reports the first measurement of the $3^2D \leftarrow 3^2P$ transition of Al in the liquid helium environment. We find that the $3^2D \leftarrow 3^2P$ excitation spectrum of Al evidences the same doubly peaked structure that has been seen in the case of electronically excited alkali atoms in bulk liquid helium. On the basis of the modeling of alkali data, it is reasonable to conclude that our doubly peaked profile, which is highly unlikely due to any splitting inherent in the atomic spectra of the Al dopants, is due to a quadrupole-like distortion of the cavity in which the solute atom resides. Thus, the dual-component peak is itself indicative of solvation. Solvation of Al is further confirmed through consideration of the blue shift and width of the spectrum in comparison with the corresponding gas-phase spectrum and in light of previous studies of solvated atomic dopants.

Modeling this system using HFD-generated potential energy surfaces that assume additivity in the Al−He_n interactions, we have revealed that spin−orbit effects due to mixing of the $1^3\Pi_{1/2}$ state with the $1^3\Sigma_{1/2}$ state would be dominated by localization of the Al valence electron in its p_z orbital. This localization is brought about by a ring of four or more helium atoms in the nodal plane of the Al p_z orbital. It has been previously postulated that from four to six He atoms would assemble around an excited 3^2P Na atom in bulk liquid helium on the nodal plane.[12] As this excited electronic configuration resembles the ground-state Al atom, we expect a similar ring of He atoms to form around the Al, as described above. Further, it is probable that the requisite number of He atoms for spin−orbit quenching ($n \geq 6$) surrounds the solvated Al atom, as its *xy* electronic component includes the additional filled $3s^2$ electron shell absent in Na, and thus would represent a wider circumference along which the He atoms could be arranged.

The study of Al atoms solvated in helium droplets has also shown that fast nonradiative quenching to the 4^2S state occurs upon electronic excitation to the 3^2D state. Previous work done with alkali atoms in bulk liquid helium[25] has provided an upper limit on helium-induced electronic quenching, finding that quenching occurs faster than the spontaneous emission lifetime (i.e., faster than several nanoseconds). Our time-resolved results allow us to say that the transfer of over 7000 cm^{-1} in the case of $3^2D \rightarrow 4^2S$ quenching in Al occurs in less than 50 ps, offering a new upper limit on quenching times for solute atoms in liquid helium.

Acknowledgment. We would like to acknowledge the assistance of Dr. Elmar Schreiber and Dr. Debrata Goswami in operating the laser system used in these experiments. We also thank Dr. Franco Dalfovo for helpful conversations and for making his density functional code available to us. U.M. gratefully acknowledges a Feodor-Lynen postdoctoral fellowship of the Alexander von Humboldt foundation. This work was carried out under the AFOSR (HEDM program) grant F-49620-98-1-0045. The Princeton Center for Ultrafast Laser Applications is supported by the New Jersey Commission of Science and Technology.

References and Notes

(1) Whaley, B. *Int. Rev. Phys. Chem.* **1994**, *13*, 41.

(2) Toennies, J. P.; Vilesov, A. *Annu. Rev. Phys. Chem.* **1998**, *49*, 1.

(3) F. Stienkemeier, F.; Higgins, J.; Callegari, C.; Kanorsky, S. I.; Ernst, W. E.; Scoles, G. *Z. Phys. D* **1996**, *38*, 253.

(4) Higgins, J.; Callegari, C.; Reho, J.; Stienkemeier, F.; Ernst, W. E.; Gutowski, M.; Scoles, G. *J. Phys. Chem. A* **1998**, *102*, 4952.

(5) Fujisaki, A.; Sano, K.; Kinoshita, T.; Yabuzaki, T. *Phys. Rev. Lett.* **1993**, *71*, 1039.

(6) Kinoshita, T.; Fukuda, K.; Yabuzaki, T. *Phys. Rev. B* **1996**, *54*, 6600.

(7) Reho, J.; Callegari, C.; Higgins, J.; Ernst, W. E.; Lehmann, K. K.; Scoles, G. *Faraday Discuss.* **1997**, *108*, 161.

(8) Reho, J.; Higgins, J.; Lehmann, K. K.; Scoles, G. Manuscript in preparation.

(9) Jakubek, Z. J.; Takami, M. *Chem. Phys. Lett.* **1997**, *265*, 653.

(10) Persson, J. L.; Hui, Q.; Jakubek, Z. J.; Nakamura, M.; Takami, M. *Phys. Rev. Lett*. **1996**, *76*, 1501.

(11) Kanorsky, S.; Weis, A.; Arndt, M.; Dziewior, R.; Hänch, T. W. *Z. Phys. B* **1995**, *98*, 371.

(12) Dupont-Roc, J. *Z. Phys. B* **1995**, *98*, 383.

(13) The presence of fluorescence in the case of the heavier alkalis can be explained by the presence of the core electrons near the node of the p orbital, which keeps the ring of He atoms at larger distances, eliminating the crossing with the ground state potential energy surface.

(14) Hui, Q.; Perssen, J. L.; Beijersbergen, J. H. M.; Takami, M. *Z. Phys. B* **1995**, *98*, 353.

(15) LePicard, S. D.; Bussery-Honvalult, B.; Rebrion-Rowe, C.; Honvault, P.; Canosa, A.; Launay, J. M.; Rowe, B. R. *J. Chem. Phys.* **1998**, *108*, 10319.

(16) Spotts, J. M.; Wong, C.-K.; Johnson, M. S.; Okumura, M. *Proceedings of the High Energy Density Matter Contractor's Conference*; USAF Phillips Laboratory: Edwards AFB, CA, 1996.
(17) Grinter, R.; Singer, R. J. *Chem. Phys*. **1987**, *113*, 87.
(18) Abe, H.; Kolb, D. M. *Ber. Bunsen-Ges. Phys. Chem.* **1983**, *87*, 523.
(19) Herbert, T.; Schriever, U.; Kolb, D. M. *Chem. Phys. Lett.* **1992**, *200*, 258.
(20) Parnis, M.; Ozin, G. A. *J. Am. Chem. Soc.* **1986**, *108*, 1699.
(21) Boatz, J. A.; Sheehy, J. A. *Proceedings of the High Eenergy Density Matter Contractor's Conference*; USAF Phillips Laboratory: Edwards AFB, CA, 1998.
(22) Carrick, P. G. 31st Joint Propulsion Conference, San Diego, CA, July 1995; Paper No. A1AA95-2893.
(23) O'Connor, D. V.; Phillips, D. *Time-correlated Single Photon Counting*; Academic Press: London, 1984.
(24) Radzig, A. A.; Smirnov, B. M. *Reference Dat aon Atoms, Molecules, and Ions*; Springer-Verlag: New York, 1985.
(25) Kinoshita, T.; Fukuda, K.; Matsura, T.; Yabuzaki, T. *Phys. Rev. A* **1996**, *53*, 4054.
(26) Douketis, C.; Scoles, G.; Marchetti, S.; Zen, M.; Thakkar, A. *J. Chem. Phys.* **1982**, *76*, 3057.
(27) Scoles, G.; et al. Unpublished results.
(28) Frisch, M. J.; Trucks, G. W.; Schlegel, H. B.; Gill, P. M. W.; Johnson, B. G.; Robb, M. A.; Cheeseman, J. R.; Keith, T.; Petersson, G. A.; Montgomery, J. A.; Raghavachari, K.; Allaham, M. A.; Zakrzewski, V. G.; Ortiz, J. V.; Foresman, J. B.; Cioslowski, J.; Stefanov, B. B.; Nanayakkara, A.; Challacobe, M.; Replogle, E. S.; Gomperts, R.; Martin, R. L.; Fox, D. J.; Binkley, J. S.; Defrees, D. J.; Baker, J.; Stewart, J. P.; Head-Gordon, M.; Gonzalez, C.; Pople, J. A. *Gaussian 94*, revision C.3; Gaussian, Inc.: Pittsburgh, PA, 1995.
(29) Standard, J. M.; Certain, P. R. *J. Chem. Phys*. **1985**, *83*, 3002.
(30) Kramer, H. L.; Herschbach, D. R. *J. Chem. Phys.* **1970**, *53*, 2792.
(31) Dalfovo, F. *Z. Phys. D* **1994**, *29*, 61.
(32) Results to be reported in a subsequent communication.
(33) Yang, X.; Dagdigian, P. J.; Alexander, M. H. *J. Chem. Phys*. **1998**, *108*, 3522.
(34) Heidecke, S. A.; Fu, Z.; Colt, J. R.; Morse, M. D. *J. Chem. Phys*. **1992**, *97*, 1692.
(35) McQuaid, M. J.; Gole, J. L.; Heaven, M. C. *J. Chem. Phys*. **1990**, *92*, 2733.
(36) Callender, C. L.; Mitchell, S. A.; Hackett, P. A. *J. Chem. Phys*. **1989**, *90*, 5252.
(37) Fu, Z.; Massick, S.; Kaup, J. G.; d'Azy, O. B.; Breckenridge, W. H. *J. Chem. Phys*. **1992**, *97*, 1683.
(38) Barnett, R. N.; Whaley, K. B. *J. Chem. Phys*. **1993**, *99*, 9738. Barnett, R. N.; Whaley, K. B. *J. Chem. Phys*. **1995**, *102*, 2290.
(39) Robkoff, H. N.; Hallock, R. B. *Phys. Rev. B* **1981**, *25*, 1572.
(40) For a He droplet the size of those employed in our experiments, the density in the region of the center is expected to approach that of the bulk liquid, so that the He−He distance could be gotten from the peak of the pair correlation known from bulk liquid helium as is done in the text. However, the inclusion of the dopant increases the local density around the cavity in which the solute atom resides', and thus the He−He distance of the He_n polygons would be expected to be *smaller* than is found from consideration of the bulk liquid.
(41) Andover Corporation, P/N 300FS40−50. This filter has a central transmission frequency of 33 333 cm^{-1} and a full-width-at-half-maximum of 4200 cm^{-1}.
(42) Calculated from Einstein coefficients given in: *Handbook of Chemistry and Physics*, 79th ed.; Lide, D. R., Ed.; CRC Press: Boca Raton, FL, 1998.
(43) Andover Corporation, P/N 400FS40−50. This filter has a central transmission frequency of 25 000 cm^{-1} and a full-width-at-half-maximum of 2620 cm^{-1}.
(44) Reho, J.; Higgins, J.; Lehmann, K. K.; Scoles, G. Unpublished results.